# Hallucinating 3D Facial Shapes

Gang Pan*, Song Han, Zhaohui Wu
College of Compute Science, Zhejiang University
{gpan,hansong1983,wzh}@zju.edu.cn

## Abstract

*This paper focuses on hallucinating a facial shape from a low-resolution 3D facial shape. Firstly, we give a constrained conformal embedding of 3D shape in $R^2$, which establishes an isomorphic mapping between curved facial surface and 2D planar domain. With such conformal embedding, two planar representations of 3D shapes are proposed:* ***Gaussian curvature image*** *(**GCI**) for a facial surface, and* ***surface displacement image*** *(**SDI**) for a pair of facial surfaces. The conformal planar representation reduces the data complexity from 3D irregular curved surface to 2D regular grid while preserving the necessary information for hallucination. Then, hallucinating a low resolution facial shape is formalized as inference of SDI from GCIs by modeling the relationship between GCI and SDI by RBF regression. The experiments on USF HumanID 3D face database demonstrate the effectiveness of the approach. Our method can be easily extended to hallucinate those category-specific 3D surfaces sharing with similar geometric structures.*

## 1. Introduction

Super-resolution is a technique which infers high resolution (*hi-res*) data from low resolution (*low-res*) data. The data could be images, videos, 3D models, audios, etc. In some references, it also is called *hallucination*[2]. It has various applications such as video surveillance, audio-video communication, object recognition, data compression, digital games. There have been a lot of methods presented in the recent decade [1, 2, 3, 4, 5, 6, 7, 8, 9, 11, 12, 13, 14, 15]. However, most of the previous work focuses on data of images and videos. Super-resolution of 3D data is little addressed.

With the fast development of 3D scanning technology, utilization of 3D models is becoming ubiquitous. Benefits of 3D super-resolution are in many aspects:

- It may overcome the limits of environments, devices and subjects that lead to reduction of data resolution during the capture of 3D data, for example, capturing only at a distance allowed, capturing the not-well-cooperative subjects. Besides, the data acquired by economic 3D scanners and fast capturing systems are usually of relatively low resolution. Thus, there are many cases that only low resolution data are available, where hallucination of low-res data is very helpful.
- It reduces 3D data volume. 3D data are usually of large size due to one more dimension than images. In addition to mesh compression[16], super-resolution of 3D data offers an alternative way to reduce data volume. In the case of transmission over Internet, we can deliver only a simplified version of the original data and rebuild the high resolution version at remote end.

This paper takes 3D human face as a typical 3D object category, and mainly focuses on hallucination of 3D facial shapes.

### 1.1. Previous Work

It is a challenging task to discover the high resolution data from a low resolution input. Most of previous work are on images or videos. For generic image super-resolution, the homogeneous Markov random field (MRF) has been widely adopted for modeling images [1, 3, 4, 6]. This kind of methods do the local feature inference on low-level vision. At a higher level, e.g. Sun et al. used a primal sketch estimated from the low resolution image to guide the edge finding[7], Dai et al employed edge smooth prior for alpha channel super-resolution [13].

The methods for generic images often do not work well in hallucinating structural visual patterns, e.g. human faces, because they ignored the special property of face images. The pioneering work on face hallucination was done by Baker et al [2]. They presented a face hallucinating algorithm using a number of training pairs to learn the statistics between the hi-res and low-res images in a nonparametric way. The hi-res features are inferred from *parent structure* by nearest neighbor searching. Wang et al developed a eigentransformation-based face hallucination approach,

*Corresponding author: Gang Pan {gpan@zju.edu.cn}

978-1-4244-2243-2/08/$25.00 ©2008 IEEE

which used principal component analysis to fit the input image as a linear combination of the low-res face images in the training set, and then the hi-res image was constructed by replacing the low-res eigen-subspace's basis with the hi-res eigen-subspace's basis while keeping the combination weights unchanged. This method is easy to manipulate but it has the defect of missing local details. To enhance facial local details, a two-step statistical approach was proposed by Liu et al [5]. It integrated a global parametric model and a local nonparametric model. Recently they improved it for practical application purpose [15]. With inspiration by Liu's effective work of two-step modeling, W.Liu et al [9] and Zhuang et al [14] presented face hallucination approaches both in the two-step framework: firstly, a global face image with main characteristics of hi-res was obtained which looks smooth and lacks some detailed features. Secondly, an optimal residue face image containing more hi-res information was added.

However, there is little work on 3D data hallucination. Peng et al first extended Baker's image-based face hallucination approach [2] to 3D facial shape. Pan et al [11] presented a progressive resolution chain (PRC) model for 3D face shapes, then developed a 3D face super-resolution approach in a MAP framework. Yang et al.[12] proposed a new post-processing step to enhance the spatial and depth resolution of low-quality and highly quantized range maps using a registered high-quality texture color image as reference. Actually it is an enhancing of 3D using 2D, while our goal is to enhance 3D using 3D.

## 2. Conformal Planar Representations of Facial Shapes

Due to irregularity of curved surface in 3D spatial space, it is a great difficulty to analyze and model 3D triangular mesh directly using their vertices, edges and triangles. Our idea is to unfold a facial surface onto a planar domain, thus we can represent a surface with a regular grid, like rasterized images. Meanwhile, we hope this representation could reduce deformation variation over different facial shapes and align their geometric structures.

This section presents two planar representations: GCI for a facial shape, SDI for a pair of facial shapes, both of which are built on constrained conformal unfolding of the facial surfaces.

### 2.1. Surface Unfolding with Constrained Conformal Embedding

According to conformal geometry theory, a 3D surface with disk topology can been isomorphically mapped to a 2D domain through a global optimization [17]. This mapping could be one-to-one, onto, and conformal. With conformal mapping, each vertex on facial surface has a unique corresponding point in the plane. The conformal parameterization have several good characteristics: 1) it is angle-preserving, which keeps line elements unchanged except for a local scaling factor. 2) it depends on the geometry itself, not the triangulation of surfaces. 3) it is easy to control.

Here, we achieve the conformal mapping by harmonic energy minimization [18]. For shape alignment purpose, we use a base mesh as a constraint and fix a few keypoints of facial mesh when performing conformal mapping. This leads to the constrained conformal embedding for surface unfolding.

For simplicity, we consider the 1-ring first. Let $S^{'}$ be a simple mesh consisting of a 1-ring neighborhood in 3D space, and let $U^{'}$ be an isomorph to $S^{'}$, shown in Fig. 1.

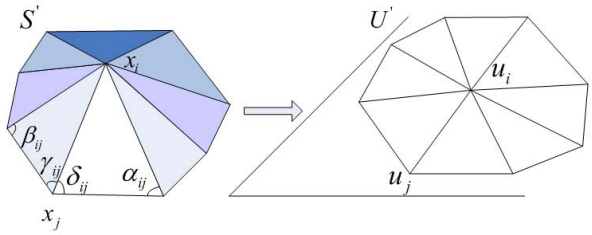


Figure 1. 3D 1-ring unfolding

Given the fixed mapping boundary, the 2D 1-ring distortion is only related to the center node $u_i$. It has been shown that Dirichlet energy is attained for angle-preserving, and could be written as [19]:

$$E_A = \sum_{j \in N(i)} cot\alpha_{ij} |u_i - u_j|^2 \tag{1}$$

where $|u_i - u_j|$ is length of the edge $(i, j)$ in $U^{'}$, $N(i)$ means 1-ring neighbor of node $i$, and $\alpha_{ij}$ is the angle shown in Fig. 1. With $\partial E / \partial u_i = 0$, the following equation could be derived:

$$\frac{\partial E}{\partial u_i} = \sum_{j \in N(i)} (cot\alpha_{ij} + cot\beta_{ij})(u_i - u_j) = 0 \tag{2}$$

For the whole facial mesh, from Equ.(2) it can be deduced that:

$$\mathcal{D}U = 0 \tag{3}$$

where $U$ is the vector of 2D-coordinates in the planar domain, and $\mathcal{D}$ is a sparse matrix given by:

$$\mathcal{D}_{ij} = \begin{cases} cot(\alpha_{ij}) + cot(\beta_{ij}) & \text{if } j \in N(i) \\ -\sum_{k \in N(i)} \mathcal{D}_{ik} & \text{if } i = j \\ 0 & \text{otherwise} \end{cases} \tag{4}$$

For the alignment purpose, we define a 3D face base mesh with 19 vertices to constrain the surface unfolding. The base mesh is shown in Fig.2.

Given the mapped boundary and fixed points in the base mesh, the unfolding system yields:

$$\tilde{\mathcal{D}}U = \begin{bmatrix} \mathcal{D} \\ 0 \quad I \end{bmatrix} \begin{bmatrix} U_{free} \\ U_{spec} \end{bmatrix} = \begin{bmatrix} 0 \\ C_{spec} \end{bmatrix} \tag{5}$$

where $U$ is separated into free points $U_{free}$ and the specified points $U_{spec}$ for convenience. This sparse linear system could be efficiently solved using generalized minimal residual algorithm[20].

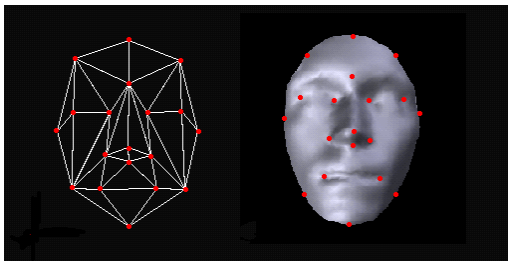

Figure 2. Three dimensional facial base mesh with 19 vertices.

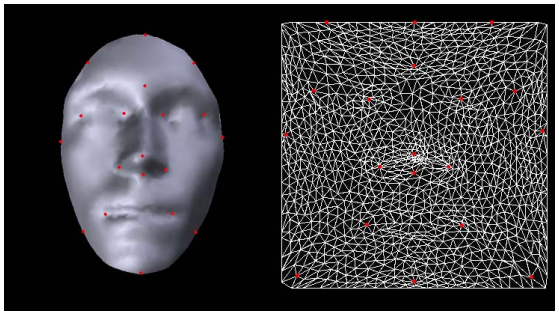

(a) (b)

Figure 3. Illustration of surface unfolding by conformal embedding. (a) The input face mesh. (b) surface unfolding result, which builds a conformal isomorphic mapping between 3D face mesh and planar unit square.

## 2.2. Gaussian Curvature Image (GCI)

Surface unfolding builds the one-to-one, onto mapping between a facial shape and a planar region, for example, a unit square. With this correspondence, if we specify an attribute for vertices in the planar region, an attributed image will be generated. This attribute should deliver some intrinsic information of the 3D surface.

Curvature is one of the most important property for shape geometry, which is invariant to Euclidean transformation. According to differential geometry theory, the local shape of a surface is completely specified by two of the principal curvatures and their directions [21]. This theorem reveals that curvature conveys intrinsic geometry information of a curved surface.

There are four kinds of curvature: two principal curvatures, mean curvature, and Gaussian curvature. In this paper, we employ Gaussian curvature as the local attribute for surface's vertex in the planar region. We only considers the curvature magnitude, although it includes magnitude and direction. The resulting planar attributed image is called *Gaussian Curvature Image* (GCI).

Gaussian curvature is defined as production of two of the principal curvatures:

$$K = k_{min} k_{max} \tag{6}$$

Given the first fundamental form and the second fundamental form of a local surface, Gaussian curvature can be computed as [22]:

$$K = \frac{eg - f^2}{EG - F^2}. \tag{7}$$

where $E, F, G$ are variables in the fist fundamental form of the surface and $e, f, g$ are in the second fundamental form.

In the discrete case, there are many approximate approach for curvature estimation over triangular mesh [23]. The Guass-Bonnet method is adopted in this paper for its accuracy and robustness. It is roughly reviewed as follows.

Consider a vertex $v$ and its immediate neighborhood $\{v_i\}_{i=0}^{n-1}$. Then, for $i = 0, ..., n-1$, let $\alpha_i = \angle(v_i, v, v_{(i+1) \mod n})$ be the angle at $v$ between two successive edges $e_i = \overrightarrow{vv_i}$. The Gauss-Bonnet theorem can be written as:

$$\int\int_A K dA = 2\pi - \sum_{i=0}^{n-1} \alpha_i \tag{8}$$

where $A$ is the accumulated areas of triangles around $v$. Gaussian curvature $K$ is approximately constant in the local neighborhood, and is then estimated as

$$K = \frac{2\pi - \sum_{i=0}^{n-1} \alpha_i}{\frac{1}{3} A} \tag{9}$$

To cope with the distribution irregularity of surface vertices in the unit square, the final GCI is obtained by resampling into a regular planar grid by bilinear interpolation. Figure 4 shows a GCI example.

## 2.3. Surface Displacement Image (SDI)

GCI gives a 2D representation for each 3D facial surface. Similarly, this section introduces a 2D representation for each pair of facial surfaces, named *Surface Displacement Image* (SDI), which measures the spatial difference between two facial shapes.

Suppose $M_1$ and $M_2$ are two facial meshes with fine registration, SDI from $M_1$ to $M_2$ is defined as

$$\mathbf{D}(M_1, M_2) = M_2 \ominus M_1 \tag{10}$$

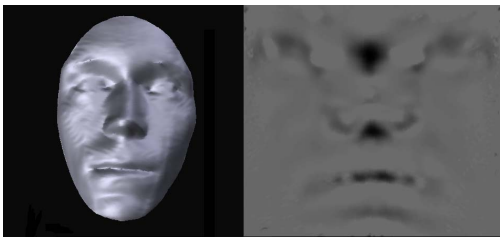

(a) (b)

Figure 4. Illustration of Gaussian Curvature Image (GCI). (a) The input facial mesh. (b) The GCI of (a) after surface unfolding onto a unit square.

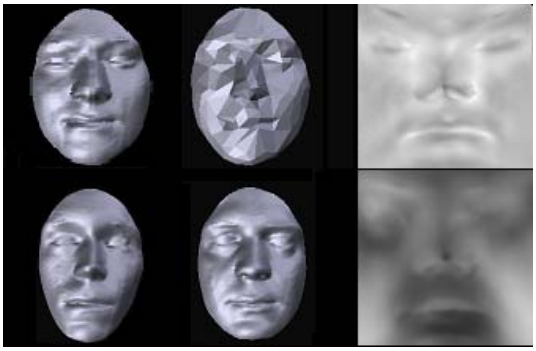

Figure 5. Surface Displacement Images (SDIs). The third column is the SDI of the first column and the second column. The first row is the SDI of a hi-res face and its low-res face. The second row is the SDI of two different individuals.

where $\ominus$ is the displacement operator. SDI is also an attributed map whose attribute is the signed difference between two facial surfaces. The displacement operator is described as follows. For each vertex $m_1^i$ on $M_1$, its corresponding vertex $m_2^{j(i)}$ on $M_2$ is calculated as the point of intersection of the line along its normal with the surface $M_2$. Then, for each vertex on $M_1$, the displacement is obtained by subtracting $m_2^{j(i)}$ from $m_1^i$.

Similar to GCI, with the displacement as the vertex attribute, an attributed image for $M_1$, called SDI, can be generated by conformal unfolding of the surface $M_1$ and resampling in the resulting planar region. Prior to computation of SDI, the facial shape pair are registered using Iterative Closest Point(ICP) method [24] first. Figure 5 shows two examples of SDIs: the first row is SDI between a high resolution mesh and the low resolution mesh of the same face, the second row is SDI between two high resolution meshes of different individuals.

## 3. Inference of SDI from GCI

We describe 3D facial shape hallucination problem as

*Given $n$ high resolution facial meshes $\{M_i^H\}_{i=1}^n$ and a low resolution facial mesh $X$, how to infer a high resolution mesh of $X$ from the training data $\{M_i^H\}_{i=1}^n$?*

From the definition of SDI, the restoration of hi-res mesh from low-res one can be written as

$$X^H = X^L \oplus \mathbf{D}(X^L, X^H) \tag{11}$$

Let $C^L$ be the GCI of $X^L$. Therefore, after representation of $X^L$ by $C^L$, the hallucination problem is converted to infer the SDI of $X^L$ from its GCI.

$$\hat{X}^H = X^L \oplus \hat{\mathbf{D}}(C^L) \tag{12}$$

As described in Sect.2, on the one hand, GCI conveys the intrinsic geometric information of the low resolution mesh, on the other hand, SDI encodes the knowledge of difference between high resolution and low resolution facial meshes. If we appropriately model the relationship between GCI and SDI, the SDI may effectively be inferred when GCI is known. In this section, we simply approximate the correlations of GCI and SDI linearly using a series of basis functions of RBF kernel.

In order to make the GCI-driven SDI inference stronger and more effective, it is necessary to highlight the intrinsic features of GCI prior to the relationship modeling. Thus, a subspace modeling of GCIs is performed in advance. We adopt the locality preserving projections (LPP) [25] for its simplicity and performance efficiency.

### 3.1. Modeling GCI Subspace by LPP

The locality preserving projections (LPP) [25] is a linear approximation of the non-linear Laplacian Eigenmap, it builds a graph incorporating neighborhood information of the data set and finds an optimal linear approximations to eigenfunction of the Laplace Beltrami operator on manifold. The advantages of LPP are: 1) it is linear, while it is capable of finding the non-linear structure of the data manifold. 2) it is defined everywhere in ambient space rather than just on the training data points.

Let $C = [C_1, ..., C_n]$, where $C_i$ is a vector representing the GCI of $M_i^L$. We perform LPP on $C$ to obtain the transformation matrix $\mathcal{Q}$. With the matrix $\mathcal{Q}$, each GCI can be projected onto the subspace spanned by row vectors of $\mathcal{Q}$.

$$\tilde{C}_i = \mathcal{Q}C_i, \tag{13}$$

The transformation matrix $\mathcal{Q}$ is solved by four steps, as described below.

1. Conduct PCA on $C$ and obtain the eigensignals $S = [s_1, ..., s_n]$ where each $s_i$ is a column vector of length $n$. ( Assuming that $dim(C_i) \gg n$ ).

2. Calculate the weight matrix $W$: for each $s_i$, find the k nearest neighbors $\{s_{i_1}, ..., s_{i_k}\}$; for each neighbor $s_j \in \{s_{i_1}, ..., s_{i_k}\}$, set $W_{ij} = \|s_i - s_j\|^2$, otherwise set $W_{ij} = 0$.

3. Generate the Laplacian matrix $L = A - W$ where $A_{ii} = \sum_j W_{ji}$.

4. Perform PCA on the matrix $SLS^T$ and select $m$ eigenvectors according to the ascending order of eigenvalues to construct the transformation matrix $\mathcal{Q}$.

### 3.2. Modeling Relationship between GCI and SDI

Let $\{(M_i^H, M_i^L)\}_{i=1}^n$ be high resolution and low resolution pairs, where $M_i^L$ denotes a low resolution version of $M_i^H$, and $D = [D_1, ..., D_n]$, where $D_i = \mathbf{D}(M_i^L, M_i^H)$, the SDI from low resolution mesh to high resolution mesh. After the dimensionality reduction by LPP, we employ RBF regress to build the relationship between GCI and SDI.

The RBF networks are able to model complex mappings and have the advantage of being much simpler than perceptrons while keeping the major property of universal approximation of functions [26]. The RBF regression algorithm is to firstly choose some proper data points as radial basis function centers and then use singular value decomposition to solve for the weights of the network [27]. The most distinguishing feature of RBF functions is that they are local, or at least their response decreases monotonically away from a central point. RBF regression has been successfully applied in image-based face hallucination [14].

The basic form of RBF is

$$D_i = \sum_{j=1}^{n} w_j k(\tilde{C}_i, \tilde{C}_j) \tag{14}$$

where

$$k(\tilde{C}_i, \tilde{C}_j) = \exp(\left\|\tilde{C}_i - \tilde{C}_j\right\|^2 / 2\sigma^2) \tag{15}$$

.

With $K_{ij} = k(\tilde{C}_i, \tilde{C}_j)$, the matrix form of RBF can be written as

$$D = W * K \tag{16}$$

where

$$W = [w_1, ..., w_n] \tag{17}$$

Given GCIs $C$ and the corresponding SDIs $D$, we can train the RBF transformation matrix $W$. When $\tilde{C}^L$, LPP of a probe $C^L$, is as an input, the corresponding SDI $\hat{D}(C^L)$ can be obtained using the matrix $W$. From Equ.12, the hallucinating hi-res version can be obtained.

### 3.3. Diagram of Hallucination Algorithm

The outline of our hallucination algorithm is shown in Fig.6. In order to make the curvature and normal estimation of low-res meshes more reasonable, Loop subdivision method [28] is at first performed on each low resolution mesh.

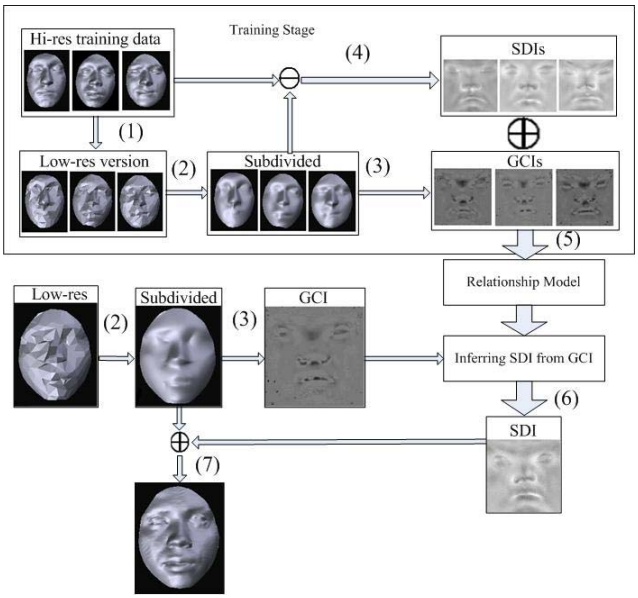


Figure 6. Algorithm outline. (1) Generation of low-res version of hi-res training data. (2) Loop subdivision. (3) Computation of GCIs. (4) Computing SDIs from hi-res meshes and their subdivided meshed. (5) Training the relationship model. (6) Inference of SDI from GCI. (7) Inverse displacement operation.

## 4. Experimental Results

### 4.1. Data and Preprocessing

We conducted the experiments using the USF Human ID 3D face database[29], which consists of 136 individuals with only one 3D model for each individual. These models are captured by *Cyberware* 3030PS laser scanner. There are more than 90,000 vertices and 180,000 faces for each model.

Original USF models include ear and neck parts. For the experiments, we extract the region-of-interest (ROI), similar to the method in [30]. The fast marching method is used to calculate each point's geodesic distance to the nose tip. We set a radius $r = 100$ and exclude those points whose distance to nose tip is larger than $r$.

For computational efficiency, the progressive mesh method [31] is adopted to simplify the ROI of each model to 16,000 vertices as our dataset of high resolution 3D face models, which preserves much details. For each obtained mesh, base mesh is labeled manually.

We adopt the leave-one-out methodology to test the performance of our algorithm, i.e., for each test, one model is chosen from the dataset as the probe, and all the other models act as the training set. Since each person has just one model in the database, for each test, the person whose model acts as the probe never appears in the corresponding training set. There are two version of the probes: the hi-res probe for the ground-truth, and the low-res one for the test

| RMS | avg. | min. | max. |
|---|---|---|---|
| $\|low\text{-}res - original\|$ | 1.408 | 0.851 | 1.847 |
| $\|subdivided - original\|$ | 1.077 | 0.951 | 1.165 |
| $\|hallucinated - original\|$ | 0.661 | 0.531 | 0.781 |

Table 1. Statistics of RMS measure for 136 models. The subdivision method uses Loop's one[28].

input. Each low-res probe mesh contains 150 vertices and about 260 triangles, simplified from hi-res probe by [31].

### 4.2. Hallucination Results

The number of LPP transformation vectors for GCI subspace modeling is set to 30 in our experiment. We adopt the root-mean-square (RMS) to quantitatively measure the effectiveness of the hallucination. RMS of two meshes $X$ and $Y$ is defined as

$$\mathbf{RMS}(X,Y) = (Dist(X,Y) + Dist(Y,X))/2 \qquad (18)$$

$$Dist(X\,Y) = \sqrt{\frac{\sum_{i=0}^{i<n} \parallel x_i - y_i \parallel^2}{n}} \qquad (19)$$

where $n$ is the vertex number of $X$, $x_i$ is a vertex of $X$, and $y_i$ is the vertex of $Y$ with the minimum distance to $x_i$.

Each test gets one RMS value. After each mode in the data set acts as the probe once, statistics of RMS is shown in Tab.1. Compared with the low-res data, average RMS between the hallucinated and the hi-res mesh drops from 1.408 to 0.661. It also significantly outperforms subdivided results.

Subdivision is the traditional resolution-enhancement method in compute graphics community. Here we compare our hallucinating results with those by two subdivision methods, one is the Loop's subdivision method [28], the other is by 3D Max, a well-known commercial professional software for 3D object modeling. Some results are shown in Fig.7. From the figure, it obviously that our hallucinating results much better than subdivision results.

## 5. Conclusion

In this paper, we propose a 3D face shape hallucination method which can restore detailed information from a low resolution input. For hallucination, we presented two planar representations: Gaussian curvature image (GCI) for a facial surface, and surface displacement image (SDI) for a pair facial surfaces. The former conveys intrinsic geometric information of the low resolution mesh, and the latter encodes the knowledge of difference between high resolution and low resolution facial mesh. With the two planar representations, the hallucination problem is converted to inference of SDI from GCI. We model the relationship between SDI and GCI by RBF regression. The experimental results on USF HumanID 3D face database, a public 3D face database, demonstrate our approach is very promising. Our framework is easily extended to hallucination of those category-specific object shapes that shares similar geometric structures.

## Acknowledgements

This work is partly supported by NSFC (60503019, 60525202), Key Program of NSFC(60533040) and PCSIRT Program (IRT0652).

## References

[1] W.Freeman, E.Pasztor, O.Carmichael. Learning low-level vision. *IJCV*, 40(1):25-47, 2000.

[2] S. Baker, T. Kanade, Hallucinating faces, *IEEE FGR'00*, pp. 83-88, 2000

[3] A.Hertzmann, C.Jacobs, N.Oliver , B.Curless, D.Salesin. Image analogies. *SIGGRAPH'01*.

[4] A.Efros, W.Freeman. Quilting for texure synthesis and transfer. *SIGGRAPH'01*.

[5] C. Liu, H. Shum, C. Zhang, A two-step approach to hallucinating faces: global parametric model and local nonparametric model, *CVPR'01*.

[6] W.Freeman, T.Jones, E.Pasztor. Example-based super-resolution. *IEEE Computer Graphics and Applications*, 22(2):56-65, 2002.

[7] J. Sun, H. Tao, H.Shum. Image Hallunication with Primal Sketch Priors. *CVPR'03*.

[8] X. Wang, X. Tang, Hallucinating face by eigentransformation, *IEEE Trans. SMC-C*, 35(3):425-434, 2005.

[9] W. Liu, D. Lin, X. Tang, Hallucinating faces: Tensorpatch super-resolution and coupled residue compensation. *CVPR'05*.

[10] S. Peng, G. Pan, Z. Wu, Learning-based Super-resolution of 3D Face Model, *IEEE ICIP'05*, vol.2, pp.382-385, Italy, September 11-14, 2005.

[11] G. Pan, S. Han, Z. Wu, Y. Wang, Super-Resolution of 3D Face, *ECCV'06*, LNCS, vol. 3952, pp.389-401, 2006.

[12] Q. Yang, R. Yang, J. Davis, D. Nister. Spatial-depth super resolution for range images. *CVPR'07*.

[13] S.Dai, M.Han, W.Xu, Y.Wu, Y.Gong, Soft Edge Smoothness Prior for Alpha Channel Super Resolution, *CVPR'07*.

[14] Y. Zhuang, J. Zhang, F. Wu, Hallucinating faces: LPH super-resolution and neighbor reconstruction for residue compensation, *Pattern Recognition*, 40(11):3178-3194, 2007.

[15] C. Liu, H. Shum, W. Freeman, Face Hallucination: Theory and Practice, *IJCV*, 75(1):115-134, 2007.

[16] J. Peng, C.S. Kim, C.C. Kuo, Technologies for 3D mesh compression: A Survey, *Journal of Visual Communication and Image Representation*, 16(6):688-733, Elsevier, 2005.

[17] A.Sheffer, E.Praun, K. Rose, Mesh parameterization methods and their applications, *Foundations and Trends in Computer Graphics and Vision*, Vol.2, Issue 2, 2006

(a) (b) (c) (d) (e)

Figure 7. Hallucinating results and comparisons. (a) The input low resolution meshes, each with 150 vertices, (b) Loop's subdivision, (c) Subdivision by *3D Max*, (d) Our hallucinating result, (e) The original high resolution meshes.

[18] M.Desbrun, M.Meyer, P.Alliez, Intrinsic Parameterizations of Surface Meshes, *EUROGRAPHICS'02*.

[19] U. Pinkall, K. Polthier, Computing Discrete Minimal Surfaces and Their Conjugates, *Experimental Mathematics*, 2(1):15-36, 1993.

[20] Y.Saad, M.Schultz, GMRES: A Generalized Minimal Residual Algorithm for Solving Nonsymmetric Linear Systems, *SIAM Journal of Scientific and Statistical Computing*, 7(3):856-869, 1986.

[21] E. Trucc, A. Verri, Introductory Techniques for 3D Computer Vision, Prentice Hall, 1998.

[22] M. do Carmo, Differential Geometry of Curves and Surfaces. Prentice Hall, 1976.

[23] T. Surazhsky, E. Magid, O. Soldea, G. Elber, E. Rivlin, A comparison of Gaussian and Mean Curvatures Estimation Methods on Triangular Meshes, *Int'l Conf. on Robotics and Automation*, 2003.

[24] P. Besl, N. McKay, A method for registration of 3D shapes, *IEEE PAMI*, Vol. 14, pp. 239-256, 1992.

[25] X. He, P. Niyogi, Locality preserving projections, *NIPS'03*.

[26] S. Chen, C. Cowan, P. Grant, Orthogonal least squares learning algorithm for radial basis function networks, IEEE Trans. Neural Networks, 2(2):302-309, 1991.

[27] T. Poggio, F. Girosi, Networks for approximation and learning, Proceedings of the IEEE, vol.78, no.9, pp.1481-1497, 1990.

[28] C.Loop, Smooth subdivision surfaces based on triangles, Master's thesis, Department of Mathematics, University of Utah, 1987

[29] V. Blanz, T. Vetter, Morphable model for the synthesis of 3D faces, *SIGGRAPH'99*.

[30] Y. Wang, G. Pan, Z. Wu, 3D Face Recognition in the Presence of Expression: A Guidance-based Constraint Deformation Approach, *CVPR'07*.

[31] H.Hoppe, Progressive meshes, *SIGGRAPH'96*.